Multi-decadal climate variability in southern Iberia during the mid- to late-Holocene

Julien Schirrmacher[1,2], Mara Weinelt[1], Thomas Blanz[3], Nils Andersen[2], Emilia Salgueiro[4], Ralph R. Schneider[1,2,3]

[1]CRC 1266, Christian-Albrechts-Universität, Kiel, 24118, Germany
5 [2]Leibniz-Laboratory for Radiometric Dating and Stable Isotope Research, Christian-Albrechts-Universität, Kiel, 24118, Germany
[3]Department of Geosciences, Christian-Albrechts-Universität, Kiel, 24118, Germany
[4]Div. Geologica e Georecursos Marinhos, Instituto Português do Mar e da Atmosfera (IPMA), Lisbon, 1749-077, Portugal

Correspondence to: Julien Schirrmacher (jschirrmacher@leibniz.uni-kiel.de)

10 **Abstract.** To assess the regional multi-decadal to multi-centennial climate variability at the southern Iberian Peninsula during the mid- to late-Holocene transition multi-proxy records of two marine sediment cores were established for two sites in the Alboran Sea (ODP-161-976A) and the Gulf of Cadiz (GeoB5901-2). High-resolution records of organic geochemical proxies and planktic foraminiferal assemblages are used to decipher precipitation and vegetation changes as well as the sea surface conditions with respect to Sea Surface Temperature (SST) and marine primary productivity (MPP). n-Alkane records as a proxy for precipitation changes suggest a series of six distinct drought events at 5.4 ka BP,
15 from ca. 5.1 ka BP to 4.9 ka BP, from 4.8 to 4.7 ka BP, at 4.6 ka BP, from 4.4 to 4.3 ka BP and, from 3.8 to 3.7 ka BP. Each drought event is associated with a major vegetation change towards higher proportions of C4 vegetation. The drought events are further accompanied by annual and spring/ winter SST warming as well as decreasing MPP in the Alboran Sea. Altogether, the close correlation of the observed droughts with North Atlantic Oscillation (NAO)-like variability suggests changes in the atmospheric circulation as important driving mechanism of terrestrial and oceanic variability at southern Iberia and the Alboran Sea, respectively. Sea surface variability in the Gulf of Cadiz, instead, is intimately
20 linked to the North Atlantic Bond Events. In particular, during Bond Events 3 and 4 a pronounced increase in seasonality is found.

1 Introduction

The Holocene has been considered to be climatically fairly stable in comparison with the large and abrupt climatic changes during the last glacial and deglacial (Dansgaard et al., 1993; Martrat et al., 2007). In the Mediterranean general long-term trends in Sea Surface Temperature (SST) cooling (Kim et al., 2004; Martrat et al., 2014) and aridification (Fletcher and Sánchez Goñi, 2008; Ramos-Román et al., 2018a) are
25 observed during the Holocene. Several climatic events superimposed to these long-term trends have been described, for example the 8.2 ka

event or the North Atlantic Bond-Events (Alley et al., 1997; Bond et al., 1997; Mayewski et al., 2004). Another prominent Holocene climate event – although not well resolved in the Greenland Ice Cores (NGRIP-Members, 2004) – is the 4.2 ka event. This event is considered of global impact with generally cooler and wetter conditions over the North Atlantic, Northern and, Central Europe broadly coincident with the onset of Neoglacial glacier advances in Scandinavia and the Alps (Bakke et al., 2010; Le Roy et al., 2017). On the other hand, severe climatic changes

5   in the tropics are described for the 4.2 ka event, for example a weakening of the African, Indian and, Asian monsoonal systems along with sudden changes in El Niño Southern Oscillation frequency (Gasse, 2000; Staubwasser et al., 2003; Toth et al., 2015). Additionally, intense drought events have been described for the mid-latitudes in Northern America and Eurasia including the Mediterranean (Booth et al., 2005; Cheng et al., 2015; Jalut et al., 2000; Magny et al., 2013). Consequently, Walker et al. (2012) proposed this event because of its global manifestation as marker separating the Middle to Late Holocene epochs. Just recently, the International Commission on Stratigraphy

10   corroborated this marker with the GSSP being a speleothem from Mawmluh Cave in India (IUGS International Commission on Stratigraphy, 2018).

The 4.2 ka climatic event is also considered to have significantly influenced the development of ancient societies in the subtropical realm. Especially evidences of sharp cultural turnover coinciding with pronounced drought in the Eastern Mediterranean and Near East gave rise to an array of collapse narratives. In particular, the collapse of the Akkadian Empire and the Old Kingdom in Egypt have been attributed to the 4.2

15   ka event (Weiss, 2017; Weiss et al., 1993; Welc and Marks, 2014). Also in the Western Mediterranean major social transformations occurred during that time (Blanco-González et al., 2018; Lillios et al., 2016). Yet, the manifestation of this climatic event and, thus, potential human responses here remain still unclear. Accordingly, clear evidences of the potential climate constraints and social transformations is still missing, though recently postulated for the western regions of the Iberian Peninsula (Blanco-González et al., 2018). This is partly related to the fact that the 4.2 ka event in the Western Mediterranean is insufficiently resolved in existing marine and terrestrial archives, e.g. several marine archives

20   show contrasting signals, thus preventing sound compilations (Weinelt et al., 2015).

Here, we explore the mid- to late- Holocene climate development in southern Iberia and, thereby, focussing on the potential manifestation and timing of the 4.2 ka event on the basis of two marine sediment cores from the Gulf of Cadiz (GeoB5901-2) and the Alboran Sea (ODP-161-976A). Both sites are analysed for terrestrial vegetation and precipitation change as well as changes in seasonal and annual SST and marine primary productivity (MPP). For that purpose, we analysed terrestrial n-alkane concentrations and specific ratios, such as Norm33 from higher

25   plant leaf-waxes for the terrestrial changes. The alkenone based SST index ($U_{37}^{K'}$) and planktic foraminiferal analyses using Modern Analogue Technique (MAT) were used to reconstruct annual and seasonal changes in SST as well as alkenone-derived MPP.

1.1 Study area

The Iberian Peninsula is influenced by two major climatic regimes: the Atlantic and the Mediterranean regime (Lionello, 2012). Today, the Atlantic climate is typically marked by relatively cool annual air temperatures and evenly distributed precipitation throughout the year. In contrast, the Mediterranean climate is generally characterized by pronounced seasonal contrasts with a rainy winter season and a dry and hot

5 summer season. In general, most of the precipitation at the Iberian Peninsula falls during the winter season (Figure 1; Lionello, 2012). The spatial pattern of winter precipitation also reflects the two climatic regimes (Figure 1). The Atlantic regime, which spans along the western and northern coasts, is characterized by high precipitation of more than 800 ml per year. The precipitation falling in the Atlantic climate is associated with the westerly wind belt at the Iberian Peninsula (Zorita et al., 1992) and is to a large extent controlled by the North Atlantic Oscillation (NAO) during winter (Hernández et al., 2015; Hurrell, 1995). During positive NAO conditions (i.e. a high pressure difference between the

10 Azores High and the Icelandic Low) the North Atlantic storm track and associated precipitation is shifted towards northern Europe, while Iberia experiences more dry conditions. On the other hand, during negative NAO conditions (i.e. a low pressure difference) more storms are directed towards the Iberian Peninsula, which experiences wetter winter conditions. Nonetheless, the central parts of the Iberian Peninsula as well as the eastern and southern coasts under influence of the Mediterranean climate remain relatively dry on average with precipitation less than 600 ml per year and also during winter during winter (Figure 1).

15 The oceanic conditions at the Atlantic margin of the Iberian Peninsula are also characterized by pronounced seasonality. Coastal upwelling along the western continental margin is responsible for relatively low SST during summer (Figure 1; Haynes et al., 1993). This upwelling system eventually spreads into the Gulf of Cadiz (Haynes et al., 1993). Warm Atlantic water passes the Strait of Gibraltar and enters the Alboran Sea. Within the Alboran Sea it circulates in two anti-cyclonic gyres (Lionello, 2012). At the western gyre relatively warm and fresh waters become upwelled (Sarhan et al., 2000). This upwelling is accompanied by an elevated MPP at the northern rim of the gyre (Minas et al., 1991).

2 Materials and methods

2.1 Sediment cores and sampling

For this study two marine sediment cores from the Alboran Sea and the Gulf of Cadiz were analysed. Sediment core ODP-161-976A (36°12.32' N; 4°18.76' W; 1108 m water depth) was retrieved in the Alboran Sea during JOIDES Resolution cruise in 1995 (Zahn et al., 1999). To achieve multi-decadal resolution, the section from 103.0 cm to 145.0 cm of the working half was continuously sampled at 0.5 cm distances. An extended

25 section from the archive half of this core (100.0 cm to 149.0 cm) was resampled on 0.5 cm resolution in the IODP Core Repository at MARUM in Bremen (Germany) to obtain additional samples for AMS^{14}C dating and planktic foraminiferal assemblage analysis. Due to an earlier

sampling of the archive half, we were just able to sample every second centimetre. Sediment core GeoB5901-2 (36°22.80' N; 7°04.28' W; 574 m water depth) was retrieved during METEOR cruise in 1999 in the Gulf of Cadiz (Schott et al., 2000). This sediment core was sampled on 0.5 cm resolution from 1.0 cm to 50.0 cm in the GeoB Core Repository at MARUM in Bremen (Germany). During this study only the section from 12.5 cm to 29.5 cm was analysed. While most of the samples from ODP-161-976A (the ones sampled in 2015) were already available freeze-

5 dried and used for organic geochemical analyses exclusively, samples of sediment core GeoB5901-2 as well as the resampled section from sediment core ODP-161-976A were subsampled for organic geochemical and foraminiferal analyses. The samples used for organic geochemical analysis were subsequently freeze-dried.

2.2 Age model

Age models of both cores are based on existing and new AMS[14]C dates, all measured at Leibniz Laboratory at Kiel University (Table 1).

10 Published data of cores ODP-161-976A and GeoB5901-2 were taken from Combourieu Nebout et al. (2002) and Kim et al. (2004), respectively. In addition, we measured six new AMS[14]C dates on monospecific planktic foraminiferal samples of *Globigerinoides ruber* white + pink or *Globigerina bulloides* larger than 150 µm from sediment core ODP-161-976A as well as seven new dates from sediment core GeoB5901-2. AMS[14]C data were calibrated and existing data recalibrated using the marine13 calibration curve and Calib7.0.4 software (Stuiver and Reimer, 1993) applying a global marine reservoir correction of 400 years. In the case of sediment core ODP-161-976A the initial age model of Jiménez-

15 Amat and Zahn (2015) through the additional age control points within the studied time period was shifted massively. In this core, for the double-dated samples yielding slightly differing ^{14}C ages at the same sample depths (120.25 cm and 132.75 cm) the age with the lowest analytical error was chosen. Two additional dates (at 116.25 cm and 124.75 cm) have been oppositely excluded, because they resulted in the same age as the sample at 120.25 cm depth (Table 1). In order to achieve the final age-depth models for both sediment cores, we linearly interpolated between the two closest AMS[14]C age control points. Accordingly, sedimentation rates range between 10.8 and 47.0 cm/kyr in core ODP-161-976A and

20 between 4.9 and 68.6 cm/kyr in core GeoB5901-2, respectively and at 0.5 sample intervals enabling thus decadal to multi-decadal resolution. The studied section of sediment core ODP-161-976A dates between 5.40 to 2.92 ka BP exhibiting a temporal resolution between 10 to 60 years per sample with continuous high resolution between 5.40 and 4.62 ka BP. The analysed section of sediment core GeoB5901-2 dates between 3.07 ka BP and 5.33 ka BP resulting in a temporal resolution between 20 and 95 years per sample. Age models and sedimentation rates for both sediment cores are shown in Figure 2.

2.3 Organic geochemical analysis and calculations

Lipids were extracted from the freeze-dried and finely ground sediment samples with an Accelerated Solvent Extractor (ASE-200, Dionex) at 100 bar and 100 °C using a 9:1 (v/v) mixture of dichloromethane (DCM) and methanol (MeOH). After extraction samples were de-sulphured by stirring for 30 minutes with activated copper. The de-sulphured lipids were subsequently separated by silica gel column chromatography

5   using activated silica gel (450 °C for 4 h) into neutral (hexane) and polar (DCM) fractions containing n-alkanes and alkenones, respectively. The neutral fraction was further separated using silver-nitrate ($AgNO_3$) coated silica gel. Samples were then left at room temperature for approximately 24 hours for homogenisation.

Afterwards, n-alkanes were analysed by gas chromatography (GC) using an Agilent 6890N gas chromatograph equipped with a Restek XTI-5 capillary column (30 m x 320 μm x 0.25 μm) and a Flame Ionization Detector (FID) at Christian-Albrechts University Kiel. n-Alkanes were

10   identified by comparison of their retention times with an external standard containing a series of n-alkane homologues of known concentration. On this basis, n-alkanes were also quantified using the FID peak areas calibrated against the external standard. For environmental interpretation the sum of terrestrial sourced, odd n-alkane homologues C_{27} to C_{33} is used. The mean analytical error (2σ) is 7.0 ng/ g sediment based on replicate analyses (n = 62).

Various studies used ratios among individual n-alkane homologues as environmental sensitive parameter, for example the Norm33 ratio (e.g.

15   (Herrmann et al., 2016). The Norm33 ratio was calculated by the following equation:

$$Norm33 = C_{33} / (C_{29} + C_{33}) \tag{1}$$

where C_X is the peak area of the n-alkane with x carbon atoms in the chromatogram. The mean analytical error (2σ) is 0.004 based on replicate analyses (n = 62).

Alkenones were analysed on a multi-dimensional, double gas column chromatography (MD-GC) set up with two Agilent 6890 gas

20   chromatographs. The compounds ($C_{37:2}$ and $C_{37:3}$) were quantified by calibration to an external standard. The alkenone concentration is derived from the sum of the $C_{37:2}$ and $C_{37:3}$ isomers. The alkenone unsaturation index ($U_{37}^{K'}$) was obtained by using the peak areas of the aforementioned compounds applying the equation of Prahl and Wakeham (1987):

$$U_{37}^{K'} = C_{37:2} / (C_{37:2} + C_{37:3}) \tag{2}$$

where C_X represents the respective peak area in the chromatogram. The $U_{37}^{K'}$ index was subsequently transferred into annual mean SST using

25   the calibration of Müller et al. (1998):

$$SST\ (°C) = (U_{37}^{K'} - 0.044) / 0.033 \tag{3}$$

The laboratory internal analytical error is approximately 0.12 °C, while the error of the calibration is 1.0 °C.

2.4 Planktic foraminiferal analysis and Modern Analogue Technique

For foraminiferal analysis sediment samples of approximately 10 ccm were washed over 63 μm sieves, dried at 40 °C and, subsequently dry sieved. Planktic foraminifera assemblages were analysed in the size fractions >150 μm enabling the application of commonly used transfer techniques for SST reconstructions based on relative abundances of 26 taxonomic categories within the assemblage, following concepts by

5   Pflaumann et al. (1996). For reliable assemblage counts samples were dry split into aliquots of at least 300 specimens with a Kiel dry sample splitter. For SST estimates we used SIMMAX non-distance-weighted modern analogue technique, using a similarity index of >0.963 and based on 10 closest analogues (Pflaumann et al., 2003). A calibration data set was used combining 1066 core top assemblages from both, the North Atlantic as compiled by the MARGO project (Hayes et al., 2005; Kucera et al., 2005a; Kucera et al., 2005b) and for the Mediterranean (Salgueiro et al., 2014). Modern temperature at 10 m water depth present-day SST was retrieved from the World Ocean Atlas 1998 (Salgueiro et al., 2014).

10   Seasonal temperatures are averaged for northern hemisphere summer (July to September) and for winter (December to February). This method as applied on core top samples yields an accuracy of better than 1 °C standard deviations for both, the Atlantic and the Mediterranean for summer and winter seasons (Hayes et al., 2005; Pflaumann et al., 2003; Salgueiro et al., 2014).

2.5 Proxy restrictions

Terrestrial n-alkanes derived from higher plant leaf waxes are commonly transported into the marine realm via aeolian and riverine transport

15   (Bird et al., 1995; Conte and Weber, 2002; Schreuder et al., 2018). The fraction of the riverine input in coastal areas is usually much higher compared to the aeolian input. Therefore, terrestrial n-alkane concentrations have already been successfully applied to study the riverine input in coastal settings in the Mediterranean (Abrantes et al., 2017; Cortina et al., 2016; Jalali et al., 2016; Jalali et al., 2017). More specifically, Rodrigo-Gámiz et al. (2015) have shown from radiogenic isotopes that in the Alboran Sea the riverine dominates the aeolian input during the studied time period. Consequently, the n-alkane concentrations analysed during this study are considered to primarily reflect the river discharge.

20   The Norm33 ratio or the proportion of the C_{33} n-alkane homologue, respectively, is a function of a change in C4 plant distribution according to air temperature and/ or precipitation change (Bush and McInerney, 2013; Herrmann et al., 2016; Leider et al., 2013; Rommerskirchen et al., 2006; Vogts et al., 2009; Vogts et al., 2012). Because of the dominant riverine transport mechanism, it is assumed that both proxies integrate spatially over the river catchment areas shown in Figure 1 and, thus, indicate climate conditions on a sub-regional level. The dominant main catchment for sediment core GeoB5901-2 is the one of the Guadalquivir river draining into the Gulf of Cadiz. The smaller mountainous rivers

25   draining the southern Sierra Nevada area are considered as more relevant for sediment core ODP-161-976A. A delivery of material from the Guadalquivir with the inflow of the Atlantic water through the Strait of Gibraltar might also be possible, though. Since the river discharge and

also the plant growing season is strongly coupled to precipitation and the rainy season at the Iberian Peninsula is in winter, both proxies are probably biased towards the winter season (Figure 1; Lionello, 2012).

3 Results

While the reconstructions from ODP-161-976A cover a period from 5.4 to 2.9 ka BP on high-resolution, the organic geochemical data from
5   GeoB5901-2 covers a slightly shorter period from 5.3 to 3.0 ka BP also on generally lower resolution. The planktic foraminiferal data from GeoB5901-2 are shown for the period from 6.0 to 2.6 ka BP.

The terrestrial n-alkane concentration vary between 67 and 714 ng/g sediment in ODP-161-976A and between 9 and 535 ng/g sediment in GeoB5901-2 (Figure 3). While in ODP-161-976A n-alkane concentrations appear generally stable and no trends are recognizable, the data from GeoB5901-2 reveal an increasing trend towards younger ages. In the later core several distinct and brief changes towards concentrations below
10   100 ng/g sediment are observed from 5.1 to 4.7, from 4.4 to 4.3 and, from 3.8 to 3.7 ka BP. In ODP-161-976A minima of similar amplitude occur at 5.4, at 4.9, from 4.8 to 4.7, at ca. 4.6 as well as at 3.7 ka BP and, thus, are generally contemporaneous. High and overall stable concentrations above 500 ng/g sediment are observed between 4.3 and 3.8 ka BP in ODP-161-976A. The Norm33 of both sediment cores show no trends varying between 0.29 and 0.49 (Figure 3). Norm33 maxima in sediment core ODP-161-976A range from 5.4 to 5.3, from 5.0 to 4.9 and, from 3.0 to 2.9 ka BP. In addition, short-lived maxima occur at ca. 4.8, at ca. 4.6 and, at 4.2 ka BP. In GeoB5901-2 Norm33 maxima occur
15   at 5.0, 4.7, 4.3 and, 3.7 ka BP.

The alkenone derived SST also exhibits relatively stable levels in both sediment cores with annual temperatures varying between 18.9 °C and 20.0 °C in ODP-161-976A and higher annual temperatures in GeoB5901-2 (20.0 °C to 22.7 °C; Figure 3). Notably, the ODP-161-976A record shows higher variability between 5.4 and 4.6 ka BP with maximal amplitudes of 1.0 °C varying around the mean of 19.4 °C. After 4.6 ka BP the mean annual SST slightly cools to very stable means of 19.1 °C. This stability is just interrupted by three short-lived maxima at 4.4, 3.7 and,
20   3.3 ka BP. From 3.0 ka BP annual SSTs increase again by about 0.5 °C. Annual mean SST in GeoB5901-2 vary stable around ca. 20.0 °C except for a pronounced warming of 2.1 °C at ca. 4.3 ka BP lasting until ca. 3.8 ka BP. The MAT-derived summer and winter SSTs also show stability in general with somewhat higher variations, though. ODP-161-976A summer SSTs show a stable mean of 22.6 °C with coolings of up to 1.0 °C at 4.9, 4.6, 4.3, 3.6 and, 3.1 ka BP. These coolings in summer are accompanied by warmings of similar amplitude in winter. In general, the winter SST varies around a mean of 15.2 °C, resulting in a stable seasonal SST difference of 7.4 °C in ODP-161-976A throughout the analysed
25   period. During the seasonal SST maxima and minima, respectively, the seasonal difference decrease to minimal values of 5.7 °C. Compared with the winter and summer SSTs fluctuations the spring SSTs appear even more stable varying around 17.6 °C. While summer SST

reconstructions of GeoB5901-2 indicate similar conditions around 22.1 °C, winter conditions are slightly warmer (16.4 °C). During summer warmings between 1-2 °C amplitude are observed at 6.0, from 5.9 to 5.6, from 5.5 to 5.4, at 4.7 and, at 4.1 ka BP. The summer warmings are accompanied by coolings of similar amplitude during winter. The seasonality slightly decreases towards younger ages from SST differences of 6.4 °C to 4.7 °C. During the summer warmings and winter coolings, respectively, the seasonal difference increases up to 9.3 °C.

5   The alkenone concentration in ODP-161-976A shows also stable conditions varying between 223 and 440 ng/g sediment with minima around 5.4, 5.2, 4.9, 4.7, 4.7 and, 3.0 ka BP. Maxima occur from 4.1 to 3.9 ka BP as well as around 3.7 ka BP (Figure 6).

Altogether, the data of both sediment cores allow the detailed comparison of seasonal climate variability in the terrestrial and marine realm during the mid- to late- Holocene in southern Iberia.

4 Discussion

10   ### 4.1 Terrestrial and marine environmental conditions in southern Iberia

The terrestrial n-alkane concentration record of GeoB5901-2 from the Gulf of Cadiz generally well matches the high resolution data of ODP-161-976A from the Alboran Sea (Figure 3). A notable difference appears at around 5.0 ka BP, when the GeoB5901-2 data records low concentrations since 5.1 ka BP, while low concentrations in ODP-161-976A appear not until 4.9 ka BP. This might be the result of dating uncertainties and/or due to the different river catchments with the ODP-161-976A data reflecting more the coastal Mediterranean climate, while

15   the GeoB5901-2 data indicates more the climate variability of the hinterland and the northern Sierra Nevada. Apart from that time lag the amplitude of changes towards lower concentrations are remarkably similar, suggesting that both archives jointly robustly record the wider regional climatic conditions of the southern Iberian Peninsula.

Since the concentration of terrestrial n-alkanes in marine sediment cores strongly depend on the amount of river discharge, we interpret the periods of very low concentrations in the studied sediment cores as dry periods. Accordingly, drought episodes occurred in southern Iberia at

20   5.4, from ca. 5.1 to 4.9, from 4.8 to 4.7, at around 4.6, from 4.4 to 4.3 and, from 3.8 to 3.7 ka BP. All of these droughts are already well documented within dating uncertainties in various records from the area (Figure 4). A widespread trend towards drier conditions since ca. 5.5 ka BP is not only described from pollen sequences in southern Iberia (Fletcher and Sánchez Goñi, 2008; Jalut et al., 2009) but is also well in phase with the end of the African Humid Period (deMenocal et al., 2000). This transition appears to be marked by an aridity event at ca. 5.5 ka BP as evidenced by speleothem data from El Refugio Cave and Grotte de Piste (Walczak et al., 2015; Wassenburg et al., 2016) and high charcoal

25   concentration in Cabo de Gata between ca. 5.4 and 5.3 ka BP, respectively. Also, a contemporaneous remarkable decrease in Mediterranean forest was noticed by Ramos-Román et al. (2018b) from 5.5 to 5.4 ka BP. Schröder et al. (2018) describe a drought event centred at ca. 5.3 ka

Climate
of the Past
Discussions

BP in Lake Medina (SW Iberia). The drought events between ca. 5.1 and 4.9, from 4.8 to 4.7 and, at ca. 4.6 ka BP observed in this study are corroborated by several regional speleothem records (Moreno et al., 2017; Walczak et al., 2015; Wassenburg et al., 2016) as well as a charcoal record from Cabo de Gata (Burjachs and Expósito, 2015). A dramatic forest decline occurred between 5.0 and 4.5 ka BP in SE Iberia (Pantaléon-Cano et al., 2003). Moderate forest declines are found in pollen records from the Alboran Sea and Elx sequence (Burjachs and Expósito, 2015;

5   Fletcher and Sánchez Goñi, 2008). The drought event from 4.4 to 4.3 ka BP broadly coincides with the 4.2 ka event observed speleothem records from the Eastern and Central Mediterranean (Cheng et al., 2015; Zanchetta et al., 2016). According to Burjachs and Expósito (2015) the forest decline at Elx starts at ca. 4.3 ka BP and, thus, within dating accuracy may be considered as synchronous. Moreover, a forest decline these authors observe at Cabo de Gata centres around 4.4 ka BP. Ramos-Román et al. (2018a) observe aridity pulses at 4.5 and 4.3 ka BP in Padul peat record from the Sierra Nevada. Additional indications for a severe drought at that time come from lithological analyses in SE Iberia

10   (Navarro-Hervás et al., 2014), a hiatus in pollen data from SW Iberia (Schröder et al., 2018) and, speleothem data (Moreno et al., 2017; Walczak et al., 2015; Wassenburg et al., 2016). The latest drought found in this study between 3.75 and 3.73 ka BP, although just lasting ca. 20 years, is described in pollen data from Elx and Villaverde (Burjachs and Expósito, 2015; Carrión et al., 2016), while pollen data from the Alboran Sea indicate a moderate forest decline (Fletcher and Sánchez Goñi, 2008). Additionally, indications for a severe dry event around 3.7 ka BP again come from speleothem data (Moreno et al., 2017; Walczak et al., 2015).

15   Notably, in our records all observed drought episodes are paralleled by Norm33 maxima (Figure 4). These maxima indicate a shift towards a higher abundance of C4 plants, which are much more adapted to drier (and warmer) conditions (e.g. Bush and McInerney, 2013). Moreover, our data gains support from Sierra Nevada bog sediments Borreguil de la Virgen and Borreguil de la Caldera (Figure 4; García-Alix et al., 2018), which also indicate an increase in C4 plant abundance during the droughts. In addition, pollen data from Elx and Padul record an increase in C4 grasses (*Poaceae*) at ca. 5.4, 5.0, 4.8, 4.4 and, 3.7 ka BP (Burjachs pers. comm., 2018; Ramos-Román et al., 2018b). Accordingly, the

20   droughts caused a dramatic vegetation shift although they occurred relatively fast within decades or even within years. This further implies that the vegetation in southern Iberia at that time was very sensitive to (winter) precipitation changes.

In contrast to the terrestrial variability our marine reconstructions suggest fairly stable conditions between 5.4 and 2.9 ka BP in the Alboran Sea and the Gulf of Cadiz (Figure 3). Alkenone derived annual mean SSTs from sediment core ODP-161-976A suggest temperatures around 19.2 °C, which are just slightly exceeding the modern annual SST of 18.0 °C (Locarnini et al., 2013). An overall cooling trend over the course of the

25   Holocene in response to decreasing insolation is known on regional as well as on global scale (e.g. Cacho et al., 2001; NGRIP-Members, 2004), thus corroborating slightly warmer SSTs during the mid- and late- Holocene. Moreover, annual mean SSTs around 19 °C at that time are also found by other studies from the Alboran Sea (Cacho et al., 2001; Martrat et al., 2014; Pérez-Folgado et al., 2003; Rodrigo-Gámiz et al., 2014). Our seasonal reconstructions vary around 15.2 °C in winter and 22.6 °C in summer. While the winter temperatures a very close to the modern

conditions (15.4 °C), summer SSTs indicate again slightly warmer conditions compared to recent SSTs (21.4 °C; Locarnini et al., 2013). Winter SSTs around 14.5 °C corroborating our results are also found by Pérez-Folgado et al. (2003), while they found warmer SSTs by about 2 °C during summer. On the other hand, our summer SST reconstructions confirm recent reconstructions from Rodrigo-Gámiz et al. (2014), who based on the long-chain diol index found summer SSTs around 22 °C. Some more subtle cooling events with SST declines of up to 1 °C occurred

5   at 4.9, 4.6, 4.3, 3.6 and, 3.1 ka BP during summer and are accompanied by warming events of similar magnitude during winter. Consequently, seasonality diminished during these periods. Unfortunately, the low temporal resolution of available reference cores from the area hampers the correlation of such brief SST events. Detailed comparison between our SST data and the MPP data reveals a correlation between warmer annual mean SSTs and decreased MPP at around 5.4, 5.2, 4.9, 4.7, 4.6, 4.4, 3.7 and, 3.0 ka BP (Figure 6). Comparison with the SSTs events observed in the seasonal reconstructions is difficult due to the lower temporal resolution. Nonetheless, it appears that also spring SST increases during

10 the MPP minima. Notably, the warming event from ca. 3.3 to 3.1 ka BP is not well reflected in the MPP data. Moreover, maximum MPP between 4.11 and 3.88 ka BP can be related with stable and relatively low annual and spring SSTs.

In the Gulf of Cadiz annual mean SSTs vary between 20.0 to 22.7 °C and are much warmer compared to recent temperatures (18.7 °C; Locarnini et al., 2013). Previous analyses of Kim et al. (2004) on the same sediment core yielded mean annual SSTs between 19 and 20 °C using a different SST calibration of Prahl et al. (1988), which would result in slightly cooler SSTs for our data as well. Annual mean SSTs around 20 °C in Gulf

15 of Cadiz were also found by Cacho et al. (2001). The here reconstructed annual mean SSTs appear actually more close to summer conditions (Figure 3). From the foraminiferal analysis we reconstruct summer SSTs around 22.1 °C, which compare well with modern summer SSTs of 21.7 °C at the location (Locarnini et al., 2013). Supportingly, Salgueiro et al. (2014) found summer SSTs around ca. 23 °C in the Gulf of Cadiz. Also the reconstructed mean winter temperatures of 16.4 °C are in good agreement with the modern SSTs of 16.0 °C (Locarnini et al., 2013). During summer warming events of 1-2 °C amplitude are observed at 5.99, from 5.86 to 5.64, from 5.49 to 5.42, at 4.65 and, at 4.11 ka BP and

20 these events are accompanied by cooling events during winter of similar amplitude. These events, notably, differ from the warm period found in the alkenone derived SST from 4.26 to 3.79 ka BP.

4.2 Possible drivers of terrestrial and marine climate variability

During modern times the NAO is responsible for much of the winter precipitation at the Iberian Peninsula (Hurrell, 1995; Zorita et al., 1992). Many studies show that NAO-like variability was also evident during the Holocene (Abrantes et al., 2017; Deininger et al., 2017; Olsen et al.,

25 2012). We here compare our drought events to a recently published North Atlantic storminess record from Filsø, Denmark (Figure 5; Goslin et al., 2018). Periods of increased storminess are indicating positive NAO-like conditions, which compare well with the drought events observed in this study. Accordingly, we conclude that the droughts observed between 5.4 and 2.9 ka BP in southern Iberia are very likely caused by

positive NAO-like conditions. It has to be cautioned, though, that other atmospheric circulation patterns like the Scandinavian and the East Atlantic pattern might also contribute to the observed precipitation changes (Abrantes et al., 2017; Hernández et al., 2015). It has also been suggested that NAO-like variability in the past is responsible for oceanic changes such as the position of the Azores front (Goslin et al., 2018; Repschläger et al., 2017) and increased upwelling as well as SST changes at the western Iberian margin (Abrantes et al., 2017). In more detail,

5 Abrantes et al. (2017) suggest that warm winters and cool summers during the Medieval Climate Anomaly are related to positive NAO-like conditions at the western Iberian margin. During the mid- to late- Holocene we cannot confirm a general link between the atmospheric and the oceanic conditions in the Gulf of Cadiz. While during the drought event between 4.4 and 4.3 ka BP our seasonal SSTs suggest no change, the alkenone-derived SST indicate a pronounced warming. On the other hand, during the drought event from 3.8 to 3.7 ka BP the Gulf of Cadiz experienced a sudden cooling in the annual mean SST, which lasted ca. 500 years. But in general, we observe two notable differences between

10 the oceanic conditions in the Gulf of Cadiz and the Alboran Sea: (1) the summer/winter SST variability in the Gulf of Cadiz is opposite resulting in a greater seasonality, while seasonality decreases during summer/winter variability in the Alboran Sea and (2) the observed warming/ cooling events in both areas are not contemporaneous although the distance between both locations is less than 250 km. This suggests very different mechanisms driving the oceanic variability in the Gulf of Cadiz and the Alboran Sea. The SST variability in the Gulf of Cadiz compares well with the stacked Ice-Rafted Debris (IRD) data from Bond et al. (2001) (Figure 5) implying that the seasonal SST variability in the Gulf of Cadiz

15 is driven by changes in the North Atlantic during Bond Events 3 and 4. Bond Event 2, on the other hand, is not visible in our SST data. Increased seasonality during mid-Holocene Bond Events so far is just described by Butruille et al. (2017) and van Nieuwenhove et al. (2018) for the Skagerrak and the northern North Atlantic, respectively. For the Subtropics our record from the Gulf of Cadiz is the first indicating increased seasonality from SST data associated with Bond Events. The Alboran Sea, instead, is not related to the SST development in the North Atlantic (i.e. Bond Events). But, the annual as well as seasonal SST development relate to the MPP, where higher annual mean temperatures are related

20 to decreased productivity (Figure 6). Also, warmings during spring, which is the main blooming season of coccoliths in the Alboran Sea (Bosc et al., 2004), relate to MPP minima. These changes are most likely caused by dynamics of the Western Alboran Gyre. Ausín et al. (2015) also proposed a coupling of a stable water column (i.e. higher SST and decreased upwelling) and low productivity in the Alboran Sea with dry conditions in southern Iberia. Indeed, our data corroborates the presence of drier conditions during SST increases in the annual mean and spring temperatures and low productivity in the Alboran Sea. Following Ausín et al. (2015) these conditions are caused by positive NAO-like conditions

25 slackening deep water formation in the Gulf of Lions and subsequently a weaker inflow of Atlantic Water through the Strait of Gibraltar. The good agreement of our drought events with the storminess data from Denmark (Goslin et al., 2018) underlines this interpretation. Consequently, NAO-like variability likely drives the oceanic variability in the Alboran Sea by altering the gyre circulation.

5 Conclusion

Our terrestrial proxies of both sediment cores agree well, revealing four drought events in southern Iberia from ca. 5.1 to 4.9, from 4.8 to 4.7, from 4.4 to 4.3 and, from 3.8 to 3.7 ka BP. The 4.2 ka event might be reflected in the drought occurring from 4.4 to 4.3 ka BP. Additional droughts are observed in the high-resolution core from the Alboran Sea at 5.4 and at 4.6 ka BP. All drought events occurred very fast within

5 decades or even within years and are accompanied by a shift towards more C4 vegetation. The droughts observed in southern Iberia are closely correlating with NAO-like variability suggesting that the atmospheric circulation was an important driver of terrestrial variability in southern Iberia. Moreover, the oceanic variability observed in the Alboran Sea with higher annual and seasonal (winter and spring) SSTs and lower MPP seems to be driven by NAO-like variability as well. According to Ausín et al. (2015) positive NAO-like conditions alter the gyre circulation by limiting the Atlantic inflow through the Strait of Gibraltar, which results in a stable water column and decreased upwelling. This oceanic

10 variability in the Alboran Sea is coinciding with droughts in southern Iberia. Contrastingly, oceanic variability in the Gulf of Cadiz shows no relation to the droughts or NAO-like variability, respectively. In fact, the Gulf of Cadiz reveals an opposite pattern compared to the Alboran Sea with summer warming and winter cooling. Also, the observed SST events in the Gulf of Cadiz and the Alboran Sea do not match temporarily implying different driving mechanisms. We found that the variability in the Gulf of Cadiz is related to Bond Events 3 and 4 in particular. Bond Event 2 is not resolved in our data. During Bond Events 3 and 4 we found a sharp increase in seasonality (i.e. summer warming and winter

15 cooling) not described for this area before.

Consequently, we found that climate variability at the southern Iberian Peninsula during the mid- to late- Holocene strongly depends on North Atlantic forcing. While a North Atlantic atmospheric variability similar to modern day NAO is responsible for terrestrial as well as oceanic changes in the Alboran Sea, oceanic variability in the Gulf of Cadiz is more related to the marine forcing in the North Atlantic (i.e. Bond Events).

20 **Data availability.** The data reported in this paper are archived in Pangaea (www.pangaea.de).

Author contribution. JS, the main author of this study (with contributions from all co-authors), performed the geochemical analyses underlying the precipitation, vegetation and, alkenones temperature reconstructions. JS also established the new age models for the two sediment cores. Planktic foraminiferal analyses underlying the seasonal SST reconstructions were provided by MW. ES provided the compiled calibration data

25 sets for the SIMMAX MAT analyses and computed SIMMAX SST. TB and RS supported the processing of the biomarker in the lab at the Institute of Geosciences (CAU Kiel) with the alkenone evaluation.

Competing interests. The authors declare that they have no conflict of interest.

References

Abrantes, F., Rodrigues, T., Rufino, M., Salgueiro, E., Oliveira, D., Gomes, S., Oliveira, P., Costa, A., Mil-Homes, M., Drago, T., and Naughton, F.: The Climate of the Common Era off the Iberian Peninsula, Climate of the Past Discussions, 1–42, doi:10.5194/cp-2017-84, 2017.

Alley, R. B., Mayewski, P. A., Sowers, T., Stuiver, M., Taylor, K. C., and Clark, P. U.: Geology: Holocene climatic instability: A prominent, widespread event 8200 yr ago, Geol, 25, 483–486, 1997.

Ausín, B., Flores, J. A., Sierro, F. J., Cacho, I., Hernández-Almeida, I., Martrat, B., and Grimalt, J. O.: Atmospheric patterns driving Holocene productivity in the Alboran Sea (Western Mediterranean): A multiproxy approach, The Holocene, 25, 583–595, doi:10.1177/0959683614565952, 2015.

Bakke, J., Dahl, S. O., Paasche, Ø., Riis Simonsen, J., Kvisvik, B., Bakke, K., and Nesje, A.: A complete record of Holocene glacier variability at Austre Okstindbreen, northern Norway: An integrated approach, Quaternary Science Reviews, 29, 1246–1262, doi:10.1016/j.quascirev.2010.02.012, 2010.

Bird, M. I., Summons, R. E., Gagan, M. K., Roksandic, Z., Dowling, L., Head, J., Keith Fifield, L., Cresswell, R. G., and Johnson, D. P.: Terrestrial vegetation change inferred from n-alkane σ13C analysis in the marine environment, Geochimica et Cosmochimica Acta, 59, 2853–2857, doi:10.1016/0016-7037(95)00160-2, 1995.

Blanco-González, A., Lillios, K. T., López-Sáez, J. A., and Drake, B. L.: Cultural, Demographic and Environmental Dynamics of the Copper and Early Bronze Age in Iberia (3300–1500 BC): Towards an Interregional Multiproxy Comparison at the Time of the 4.2 ky BP Event, J World Prehist, 31, 1–79, doi:10.1007/s10963-018-9113-3, 2018.

Bond, G., Kromer, B., Beer, J., Muscheler, R., Evans, M. N., Showers, W., Hoffmann, S., Lotti-Bond, R., Hajdas, I., and Bonani, G.: Persistent solar influence on North Atlantic climate during the Holocene, Science (New York, N.Y.), 294, 2130–2136, doi:10.1126/science.1065680, 2001.

Bond, G., Showers, W., Cheseby, M., Lotti, R., Almasi, P., deMenocal, P., Priore, P., Cullen, H., Hajdas, I., and Bonani, G.: A Pervasive

5   Millennial-Scale Cycle in North Atlantic Holocene and Glacial Climates, Science, 278, 1257–1266, doi:10.1126/science.278.5341.1257, 1997.

Booth, R. K., Jackson, S. T., Forman, S. L., Kutzbach, J. E., Bettis, E. A., Kreigs, J., and Wright, D. K.: A severe centennial-scale drought in midcontinental North America 4200 years ago and apparent global linkages, The Holocene, 15, 321–328, doi:10.1191/0959683605hl825ft, 2005.

10   Bosc, E., Bricaud, A., and Antoine, D.: Seasonal and interannual variability in algal biomass and primary production in the Mediterranean Sea, as derived from 4 years of SeaWiFS observations, Global Biogeochem. Cycles, 18, n/a-n/a, doi:10.1029/2003GB002034, 2004.

Burjachs, F. and Expósito, I.: Charcoal and pollen analysis: Examples of Holocene fire dynamics in Mediterranean Iberian Peninsula, CATENA, 135, 340–349, doi:10.1016/j.catena.2014.10.006, 2015.

Burjachs, F., Giralt, S., Roca, J. R., Seret, G., and Julià, R.: Palinología holocénica y desertización en el Mediterráneo occidental., in: El

15   paisaje mediterráneo a través del espacio y del tiempo.: Implicaiones en la desertificación., Ibañez, J. J., Valero, B. L., Machado, C. (Eds.), Geoforma Editores, Logroño, 379–394, 1997.

Bush, R. T. and McInerney, F. A.: Leaf wax n-alkane distributions in and across modern plants: Implications for paleoecology and chemotaxonomy, Geochimica et Cosmochimica Acta, 117, 161–179, doi:10.1016/j.gca.2013.04.016, 2013.

Butruille, C., Krossa, V. R., Schwab, C., and Weinelt, M.: Reconstruction of mid- to late-Holocene winter temperatures in the Skagerrak

20   region using benthic foraminiferal Mg/Ca and δ 18 O, The Holocene, 27, 63–72, doi:10.1177/0959683616652701, 2017.

Cacho, I., Grimalt, J. O., Canals, M., Sbaffi, L., Shackleton, N. J., Schönfeld, J., and Zahn, R.: Variability of the western Mediterranean Sea surface temperature during the last 25,000 years and its connection with the Northern Hemisphere climatic changes, Paleoceanography, 16, 40–52, doi:10.1029/2000PA000502, 2001.

Carrión, J. S., Sánchez-Gómez, P., Mota, J. F., Yll, R., and Chaín, C.: Holocene vegetation dynamics, fire and grazing in the Sierra de Gádor,

25   southern Spain, The Holocene, 13, 839–849, doi:10.1191/0959683603hl662rp, 2016.

Cheng, H., Sinha, A., Verheyden, S., Nader, F. H., Li, X. L., Zhang, P. Z., Yin, J. J., Yi, L., Peng, Y. B., Rao, Z. G., Ning, Y. F., and Edwards, R. L.: The climate variability in northern Levant over the past 20,000 years, Geophysical Research Letters, 42, 8641–8650, doi:10.1002/2015GL065397, 2015.

14

Combourieu Nebout, N., Turon, J. L., Zahn, R., Capotondi, L., Londeix, L., and Pahnke, K.: Enhanced aridity and atmospheric high-pressure
    stability over the western Mediterranean during the North Atlantic cold events of the past 50 k.y, Geol, 30, 863, doi:10.1130/0091-
    7613(2002)030<0863:EAAAHP>2.0.CO;2, 2002.

Conte, M. H. and Weber, J. C.: Long-range atmospheric transport of terrestrial biomarkers to the western North Atlantic, Global Biogeochem.
5   Cycles, 16, 89-1-89-17, doi:10.1029/2002GB001922, 2002.

Cortina, A., Grimalt, J. O., Rigual-Hernández, A., Ballegeer, A.-M., Martrat, B., Sierro, F. J., and Flores, J. A.: The impact of ice-sheet
    dynamics in western Mediterranean environmental conditions during Terminations. An approach based on terrestrial long chain n-alkanes
    deposited in the upper slope of the Gulf of Lions, Chemical Geology, 430, 21–33, doi:10.1016/j.chemgeo.2016.03.015, 2016.

Dansgaard, W., Johnsen, S. J., Clausen, H. B., Dahl-Jensen, D., Gundestrup, N. S., Hammer, C. U., Hvidberg, C. S., Steffensen, J. P.,
10   Sveinbjörnsdottir, A. E., Jouzel, J., and Bond, G.: Evidence for general instability of past climate from a 250-kyr ice-core record, Nature,
    364, 218–220, doi:10.1038/364218a0, 1993.

Deininger, M., McDermott, F., Mudelsee, M., Werner, M., Frank, N., and Mangini, A.: Coherency of late Holocene European speleothem
    δ^{18}O records linked to North Atlantic Ocean circulation, Climate Dynamics, 49, 595–618, doi:10.1007/s00382-016-3360-8, 2017.

deMenocal, P., Ortiz, J., Guilderson, T., Adkins, J., Sarnthein, M., Baker, L., and Yarusinsky, M.: Abrupt onset and termination of the African
15   Humid Period, Quaternary Science Reviews, 19, 347–361, doi:10.1016/S0277-3791(99)00081-5, 2000.

Fick, S. E. and Hijmans, R. J.: WorldClim 2: New 1-km spatial resolution climate surfaces for global land areas, Int. J. Climatol., 37, 4302–
    4315, doi:10.1002/joc.5086, 2017.

Fletcher, W. J. and Sánchez Goñi, M. F.: Orbital- and sub-orbital-scale climate impacts on vegetation of the western Mediterranean basin over
    the last 48,000 yr, Quat. res., 70, 451–464, doi:10.1016/j.yqres.2008.07.002, 2008.

20 García-Alix, A., Jiménez-Espejo, F. J., Jiménez-Moreno, G., Toney, J. L., Ramos-Román, M. J., Camuera, J., Anderson, R. S., Delgado-
    Huertas, A., Martínez-Ruiz, F., and Queralt, I.: Holocene geochemical footprint from Semi-arid alpine wetlands in southern Spain,
    Scientific data, 5, 180024, doi:10.1038/sdata.2018.24, 2018.

Gasse, F.: Hydrological changes in the African tropics since the Last Glacial Maximum, Quaternary Science Reviews, 19, 189–211,
    doi:10.1016/S0277-3791(99)00061-X, 2000.

25 Goslin, J., Fruergaard, M., Sander, L., Gałka, M., Menviel, L., Monkenbusch, J., Thibault, N., and Clemmensen, L. B.: Holocene centennial to
    millennial shifts in North-Atlantic storminess and ocean dynamics, Scientific reports, 8, 12778, doi:10.1038/s41598-018-29949-8, 2018.

Hayes, A., Kucera, M., Kallel, N., Sbaffi, L., and Rohling, E. J.: Glacial Mediterranean sea surface temperatures based on planktonic
    foraminiferal assemblages, Quaternary Science Reviews, 24, 999–1016, doi:10.1016/j.quascirev.2004.02.018, 2005.

Haynes, R., Barton, E. D., and Pilling, I.: Development, persistence, and variability of upwelling filaments off the Atlantic coast of the Iberian
    Peninsula, J. Geophys. Res., 98, 22681, doi:10.1029/93JC02016, 1993.

Hernández, A., Trigo, R. M., Pla-Rabes, S., Valero-Garcés, B. L., Jerez, S., Rico-Herrero, M., Vega, J. C., Jambrina-Enríquez, M., and Giralt,
    S.: Sensitivity of two Iberian lakes to North Atlantic atmospheric circulation modes, Clim Dyn, 45, 3403–3417, doi:10.1007/s00382-015-
5   2547-8, 2015.

Herrmann, N., Boom, A., Carr, A. S., Chase, B. M., Granger, R., Hahn, A., Zabel, M., and Schefuß, E.: Sources, transport and deposition of
    terrestrial organic material: A case study from southwestern Africa, Quaternary Science Reviews, 149, 215–229,
    doi:10.1016/j.quascirev.2016.07.028, 2016.

Hurrell, J. W.: Decadal trends in the north atlantic oscillation: regional temperatures and precipitation, Science, 269, 676–679,
10 doi:10.1126/science.269.5224.676, 1995.

IUGS International Commission on Stratigraphy: IUGS E-Bulletin, 143, 10 pp., 2018.

Jalali, B., Sicre, M.-A., Bassetti, M.-A., and Kallel, N.: Holocene climate variability in the North-Western Mediterranean Sea (Gulf of Lions),
    Climate of the Past, 12, 91–101, doi:10.5194/cp-12-91-2016, 2016.

Jalali, B., Sicre, M.-A., Kallel, N., Azuara, J., Combourieu-Nebout, N., Bassetti, M.-A., and Klein, V.: High-resolution Holocene climate and
15 hydrological variability from two major Mediterranean deltas (Nile and Rhone), The Holocene, 27, 1158–1168,
    doi:10.1177/0959683616683258, 2017.

Jalut, G., Dedoubat, J. J., Fontugne, M., and Otto, T.: Holocene circum-Mediterranean vegetation changes: Climate forcing and human
    impact, Quaternary International, 200, 4–18, doi:10.1016/j.quaint.2008.03.012, 2009.

Jalut, G., Esteban Amat, A., Bonnet, L., Gauquelin, T., and Fontugne, M.: Holocene climatic changes in the Western Mediterranean, from
20 south-east France to south-east Spain, Palaeogeography, Palaeoclimatology, Palaeoecology, 160, 255–290, doi:10.1016/S0031-
    0182(00)00075-4, 2000.

Jiménez-Amat, P. and Zahn, R.: Offset timing of climate oscillations during the last two glacial-interglacial transitions connected with large-
    scale freshwater perturbation, Paleoceanography, 30, 768–788, doi:10.1002/2014PA002710, 2015.

Kim, J.-H., Rimbu, N., Lorenz, S. J., Lohmann, G., Nam, S.-I., Schouten, S., Rühlemann, C., and Schneider, R. R.: North Pacific and North
25 Atlantic sea-surface temperature variability during the Holocene, Quaternary Science Reviews, 23, 2141–2154,
    doi:10.1016/j.quascirev.2004.08.010, 2004.

Kucera, M., Rosell-Melé, A., Schneider, R., Waelbroeck, C., and Weinelt, M.: Multiproxy approach for the reconstruction of the glacial ocean
    surface (MARGO), Quaternary Science Reviews, 24, 813–819, doi:10.1016/j.quascirev.2004.07.017, 2005a.

Kucera, M., Weinelt, M., Kiefer, T., Pflaumann, U., Hayes, A., Weinelt, M., Chen, M.-T., Mix, A. C., Barrows, T. T., Cortijo, E., Duprat, J., Juggins, S., and Waelbroeck, C.: Reconstruction of sea-surface temperatures from assemblages of planktonic foraminifera: Multi-technique approach based on geographically constrained calibration data sets and its application to glacial Atlantic and Pacific Oceans, Quaternary Science Reviews, 24, 951–998, doi:10.1016/j.quascirev.2004.07.014, 2005b.

5   Le Roy, M., Deline, P., Carcaillet, J., Schimmelpfennig, I., and Ermini, M.: 10 Be exposure dating of the timing of Neoglacial glacier advances in the Ecrins-Pelvoux massif, southern French Alps, Quaternary Science Reviews, 178, 118–138, doi:10.1016/j.quascirev.2017.10.010, 2017.

Leider, A., Hinrichs, K.-U., Schefuß, E., and Versteegh, G. J.M.: Distribution and stable isotopes of plant wax derived n-alkanes in lacustrine, fluvial and marine surface sediments along an Eastern Italian transect and their potential to reconstruct the hydrological cycle,
10   Geochimica et Cosmochimica Acta, 117, 16–32, doi:10.1016/j.gca.2013.04.018, 2013.

Lillios, K. T., Blanco-González, A., Drake, B. L., and López-Sáez, J. A.: Mid-late Holocene climate, demography, and cultural dynamics in Iberia: A multi-proxy approach, Quaternary Science Reviews, 135, 138–153, doi:10.1016/j.quascirev.2016.01.011, 2016.

Lionello, P. (Ed.): The climate of the Mediterranean region: From the past to the future, 1. ed., Elsevier insights, Elsevier Science, Amsterdam, 502 pp., 2012.

15   Locarnini, R. A., Mishonov, A. V., Antonov, J. I., Boyer, T. P., Garcia, H. E., Baranova, O. K., Zweng, M. M., Paver, C. R., Reagan, J. R., Johnson, D. R., Hamilton, M., and Seidov, D.: World Ocean Atlas 2013: Volume 1: Temperature, NOAA Atlas NESDIS 73, 40 pp., 2013.

Magny, M., Combourieu-Nebout, N., Beaulieu, J. L. de, Bout-Roumazeilles, V., Colombaroli, D., Desprat, S., Francke, A., Joannin, S., Ortu, E., Peyron, O., Revel, M., Sadori, L., Siani, G., Sicre, M. A., Samartin, S., Simonneau, A., Tinner, W., Vannière, B., Wagner, B.,
20   Zanchetta, G., Anselmetti, F., Brugiapaglia, E., Chapron, E., Debret, M., Desmet, M., Didier, J., Essallami, L., Galop, D., Gilli, A., Haas, J. N., Kallel, N., Millet, L., Stock, A., Turon, J. L., and Wirth, S.: North-south palaeohydrological contrasts in the central Mediterranean during the Holocene: Tentative synthesis and working hypotheses, Climate of the Past, 9, 2043–2071, doi:10.5194/cp-9-2043-2013, 2013.

Martrat, B., Grimalt, J. O., Shackleton, N. J., Abreu, L. de, Hutterli, M. A., and Stocker, T. F.: Four climate cycles of recurring deep and surface water destabilizations on the Iberian margin, Science (New York, N.Y.), 317, 502–507, doi:10.1126/science.1139994, 2007.

25   Martrat, B., Jiménez-Amat, P., Zahn, R., and Grimalt, J. O.: Similarities and dissimilarities between the last two deglaciations and interglaciations in the North Atlantic region, Quaternary Science Reviews, 99, 122–134, doi:10.1016/j.quascirev.2014.06.016, 2014.

17

Mayewski, P. A., Rohling, E. E., Curt Stager, J., Karlén, W., Maasch, K. A., Meeker, L. D., Meyerson, E. A., Gasse, F., van Kreveld, S., Holmgren, K., Lee-Thorp, J., Rosqvist, G., Rack, F., Staubwasser, M., Schneider, R. R., and Steig, E. J.: Holocene Climate Variability, Quat. res., 62, 243–255, doi:10.1016/j.yqres.2004.07.001, 2004.

Minas, H. J., Coste, B., Le Corre, P., Minas, M., and Raimbault, P.: Biological and geochemical signatures associated with the water
5   circulation through the Strait of Gibraltar and in the western Alboran Sea, J. Geophys. Res., 96, 8755, doi:10.1029/91JC00360, 1991.

Moreno, A., Pérez-Mejías, C., Bartolomé, M., Sancho, C., Cacho, I., Stoll, H., Delgado-Huertas, A., Hellstrom, J., Edwards, R. L., and Cheng, H.: New speleothem data from Molinos and Ejulve caves reveal Holocene hydrological variability in northeast Iberia, Quat. res., 88, 223–233, doi:10.1017/qua.2017.39, 2017.

Müller, P. J., Kirst, G., Ruhland, G., Storch, I. von, and Rosell-Melé, A.: Calibration of the alkenone paleotemperature index U37K′ based on
10   core-tops from the eastern South Atlantic and the global ocean (60°N-60°S), Geochimica et Cosmochimica Acta, 62, 1757–1772, doi:10.1016/S0016-7037(98)00097-0, 1998.

Navarro-Hervás, F., Ros-Salas, M.-M., Rodríguez-Estrella, T., Fierro-Enrique, E., Carrión, J.-S., García-Veigas, J., Flores, J.-A., Bárcena, M. Á., and García, M. S.: Evaporite evidence of a mid-Holocene (c 4550–4400 cal. yr BP) aridity crisis in southwestern Europe and palaeoenvironmental consequences, The Holocene, 24, 489–502, doi:10.1177/0959683613520260, 2014.

15 NGRIP-Members: High-resolution record of Northern Hemisphere climate extending into the last interglacial period, Nature, 431, 147–151, doi:10.1038/nature02805, 2004.

Olsen, J., Anderson, N. J., and Knudsen, M. F.: Variability of the North Atlantic Oscillation over the past 5,200 years, Nature Geoscience, 5, 808–812, doi:10.1038/ngeo1589, 2012.

Pantaléon-Cano, J., Yll, E.-I., Pérez-Obiol, R., and Roure, J. M.: Palynological evidence for vegetational history in semi-arid areas of the
20   western Mediterranean (Almería, Spain), The Holocene, 13, 109–119, doi:10.1191/0959683603hl598rp, 2003.

Pérez-Folgado, M., Sierro, F. J., Flores, J. A., Cacho, I., Grimalt, J. O., Zahn, R., and Shackleton, N.: Western Mediterranean planktonic foraminifera events and millennial climatic variability during the last 70 kyr, Marine Micropaleontology, 48, 49–70, doi:10.1016/S0377-8398(02)00160-3, 2003.

Pflaumann, U., Duprat, J., Pujol, C., and Labeyrie, L. D.: SIMMAX: A modern analog technique to deduce Atlantic sea surface temperatures
25   from planktonic foraminifera in deep-sea sediments, Paleoceanography, 11, 15–35, doi:10.1029/95PA01743, 1996.

Pflaumann, U., Sarnthein, M., Chapman, M., d'Abreu, L., Funnell, B., Huels, M., Kiefer, T., Maslin, M., Schulz, H., Swallow, J., van Kreveld, S., Vautravers, M., Vogelsang, E., and Weinelt, M.: Glacial North Atlantic: Sea-surface conditions reconstructed by GLAMAP 2000, Paleoceanography, 18, n/a-n/a, doi:10.1029/2002PA000774, 2003.

Prahl, F. G., Muehlhausen, L. A., and Zahnle, D. L.: Further evaluation of long-chain alkenones as indicators of paleoceanographic conditions, Geochimica et Cosmochimica Acta, 52, 2303–2310, doi:10.1016/0016-7037(88)90132-9, 1988.

Prahl, F. G. and Wakeham, S. G.: Calibration of unsaturation patterns in long-chain ketone compositions for palaeotemperature assessment, Nature, 330, 367–369, doi:10.1038/330367a0, 1987.

5 Ramos-Román, M. J., Jiménez-Moreno, G., Camuera, J., García-Alix, A., Anderson, R. S., Jiménez-Espejo, F. J., and Carrión, J. S.: Holocene climate aridification trend and human impact interrupted by millennial- and centennial-scale climate fluctuations from a new sedimentary record from Padul (Sierra Nevada, southern Iberian Peninsula), Clim. Past, 14, 117–137, doi:10.5194/cp-14-117-2018, 2018a.

Ramos-Román, M. J., Jiménez-Moreno, G., Camuera, J., García-Alix, A., Scott Anderson, R., Jiménez-Espejo, F. J., Sachse, D., Toney, J. L., Carrión, J. S., Webster, C., and Yanes, Y.: Millennial-scale cyclical environment and climate variability during the Holocene in the

10 western Mediterranean region deduced from a new multi-proxy analysis from the Padul record (Sierra Nevada, Spain), Global and Planetary Change, 168, 35–53, doi:10.1016/j.gloplacha.2018.06.003, 2018b.

Repschläger, J., Garbe-Schönberg, D., Weinelt, M., and Schneider, R.: Holocene evolution of the North Atlantic subsurface transport, Climate of the Past, 13, 333–344, doi:10.5194/cp-13-333-2017, 2017.

Rodrigo-Gámiz, M., Martínez-Ruiz, F., Chiaradia, M., Jiménez-Espejo, F. J., and Ariztegui, D.: Radiogenic isotopes for deciphering

15 terrigenous input provenance in the western Mediterranean, Chemical Geology, 410, 237–250, doi:10.1016/j.chemgeo.2015.06.004, 2015.

Rodrigo-Gámiz, M., Martínez-Ruiz, F., Rampen, S. W., Schouten, S., and Sinninghe Damsté, J. S.: Sea surface temperature variations in the western Mediterranean Sea over the last 20 kyr: A dual-organic proxy (U K′37 and LDI) approach, Paleoceanography, 29, 87–98, doi:10.1002/2013PA002466, 2014.

Rommerskirchen, F., Plader, A., Eglinton, G., Chikaraishi, Y., and Rullkötter, J.: Chemotaxonomic significance of distribution and stable

20 carbon isotopic composition of long-chain alkanes and alkan-1-ols in C_4 grass waxes, Organic Geochemistry, 37, 1303–1332, doi:10.1016/j.orggeochem.2005.12.013, 2006.

Salgueiro, E., Naughton, F., Voelker, A.H.L., Abreu, L. de, Alberto, A., Rossignol, L., Duprat, J., Magalhães, V. H., Vaqueiro, S., Turon, J.-L., and Abrantes, F.: Past circulation along the western Iberian margin: A time slice vision from the Last Glacial to the Holocene, Quaternary Science Reviews, 106, 316–329, doi:10.1016/j.quascirev.2014.09.001, 2014.

25 Sarhan, T., Lafuente, J. G., Vargas, M., Vargas, J. M., and Plaza, F.: Upwelling mechanisms in the northwestern Alboran Sea, Journal of Marine Systems, 23, 317–331, doi:10.1016/S0924-7963(99)00068-8, 2000.

Schlitzer, R.: Ocean Data View, 2016.

Schott, F., Meincke, J., Meinecke, G., Neuer, S., and Zenk, W.: North Atlantic 1999 - Cruise No. M45 - May 18 - November 4, 1999 - Malaga (Spain) - Las Palmas (Spain), 2000.

Schreuder, L. T., Stuut, J.-B. W., Korte, L. F., Sinninghe Damsté, J. S., and Schouten, S.: Aeolian transport and deposition of plant wax n -alkanes across the tropical North Atlantic Ocean, Organic Geochemistry, 115, 113–123, doi:10.1016/j.orggeochem.2017.10.010, 2018.

5   Schröder, T., van't Hoff, J., López-Sáez, J. A., Viehberg, F., Melles, M., and Reicherter, K.: Holocene climatic and environmental evolution on the southwestern Iberian Peninsula: A high-resolution multi-proxy study from Lake Medina (Cádiz, SW Spain), Quaternary Science Reviews, 198, 208–225, doi:10.1016/j.quascirev.2018.08.030, 2018.

Staubwasser, M., Sirocko, F., Grootes, P. M., and Segl, M.: Climate change at the 4.2 ka BP termination of the Indus valley civilization and Holocene south Asian monsoon variability, Geophysical Research Letters, 30, 155, doi:10.1029/2002GL016822, 2003.

10 Stuiver, M. and Reimer, P. J.: Extended 14C Data Base and Revised CALIB 3.0 14C Age Calibration Program, Radiocarbon, 35, 215–230, doi:10.1017/S0033822200013904, 1993.

Toth, L. T., Aronson, R. B., Cheng, H., and Edwards, R. L.: Holocene variability in the intensity of wind-gap upwelling in the tropical eastern Pacific, Paleoceanography, 30, 1113–1131, doi:10.1002/2015PA002794, 2015.

van Nieuwenhove, N., Pearce, C., Knudsen, M. F., Røy, H., and Seidenkrantz, M.-S.: Meltwater and seasonality influence on Subpolar Gyre
15 circulation during the Holocene, Palaeogeography, Palaeoclimatology, Palaeoecology, 502, 104–118, doi:10.1016/j.palaeo.2018.05.002, 2018.

Vogts, A., Moossen, H., Rommerskirchen, F., and Rullkötter, J.: Distribution patterns and stable carbon isotopic composition of alkanes and alkan-1-ols from plant waxes of African rain forest and savanna C_3 species, Organic Geochemistry, 40, 1037–1054, doi:10.1016/j.orggeochem.2009.07.011, 2009.

20 Vogts, A., Schefuß, E., Badewien, T., and Rullkötter, J.: n-Alkane parameters from a deep sea sediment transect off southwest Africa reflect continental vegetation and climate conditions, Organic Geochemistry, 47, 109–119, doi:10.1016/j.orggeochem.2012.03.011, 2012.

Walczak, I. W., Baldini, J. U.L., Baldini, L. M., McDermott, F., Marsden, S., Standish, C. D., Richards, D. A., Andreo, B., and Slater, J.: Reconstructing high-resolution climate using CT scanning of unsectioned stalagmites: A case study identifying the mid-Holocene onset of the Mediterranean climate in southern Iberia, Quaternary Science Reviews, 127, 117–128, doi:10.1016/j.quascirev.2015.06.013, 2015.

25 Walker, M. J. C., Berkelhammer, M., Björck, S., Cwynar, L. C., Fisher, D. A., Long, A. J., Lowe, J. J., Newnham, R. M., Rasmussen, S. O., and Weiss, H.: Formal subdivision of the Holocene Series/Epoch: A Discussion Paper by a Working Group of INTIMATE (Integration of ice-core, marine and terrestrial records) and the Subcommission on Quaternary Stratigraphy (International Commission on Stratigraphy), J. Quaternary Sci., 27, 649–659, doi:10.1002/jqs.2565, 2012.

Wassenburg, J. A., Dietrich, S., Fietzke, J., Fohlmeister, J., Jochum, K. P., Scholz, D., Richter, D. K., Sabaoui, A., Spötl, C., Lohmann, G., Andreae, M. O., and Immenhauser, A.: Reorganization of the North Atlantic Oscillation during early Holocene deglaciation, Nature Geoscience, 9, 602–605, doi:10.1038/ngeo2767, 2016.

Weinelt, M., Schwab, C., Kneisel, J., and Hinz, M.: Climate and societal change in the western Mediterranean area around 4.2 ka BP, in: 2200
5   BC - ein Klimasturz als Ursache für den Zerfall der alten Welt?: 7. Mitteldeutscher Archäologentag vom 23. bis 26. Oktober 2014 in Halle (Saale), Meller, H., Arz, H. W., Jung, R., Risch, R. (Eds.), Tagungen des Landesmuseums für Vorgeschichte Halle, Band 12,1, Landesamt für Denkmalpflege und Archäologie Sachsen-Anhalt, Landesmuseum für Vorgeschichte, Halle (Saale), Halle (Saale), 461–480, 2015.

Weiss, H.: 4.2 ka BP Megadrought and the Akkadian Collapse, in: Megadrought and collapse: From early agriculture to angkor, Weiss, H.
10   (Ed.), Oxford University Press, New York, NY, 93–161, 2017.

Weiss, H., Courty, M. A., Wetterstrom, W., Guichard, F., Senior, L., Meadow, R., and Curnow, A.: The genesis and collapse of third millennium north mesopotamian civilization, Science (New York, N.Y.), 261, 995–1004, doi:10.1126/science.261.5124.995, 1993.

Welc, F. and Marks, L.: Climate change at the end of the Old Kingdom in Egypt around 4200 BP: New geoarchaeological evidence, Quaternary International, 324, 124–133, doi:10.1016/j.quaint.2013.07.035, 2014.

15   Zahn, R., Comas, M. C., and Klaus, A.: Proceedings of the Ocean Drilling Program, 161 Scientific Results, 161, Ocean Drilling Program, 1999.

Zanchetta, G., Regattieri, E., Isola, I., Drysdale, R. N., Bini, M., Baneschi, I., and Hellstrom, J. C.: The so-called "4.2 event" in the Central Mediterranean and its climatic teleconnections, Alpine and Mediterranean Quaternary, 29, 5–17, 2016.

Zorita, E., Kharin, V., and Storch, H. von: The Atmospheric Circulation and Sea Surface Temperature in the North Atlantic Area in Winter:
20   Their Interaction and Relevance for Iberian Precipitation, Journal of Climate, 5, 1097–1108, doi:10.1175/1520-0442(1992)005<1097:TACASS>2.0.CO;2, 1992.

Climate
of the Past
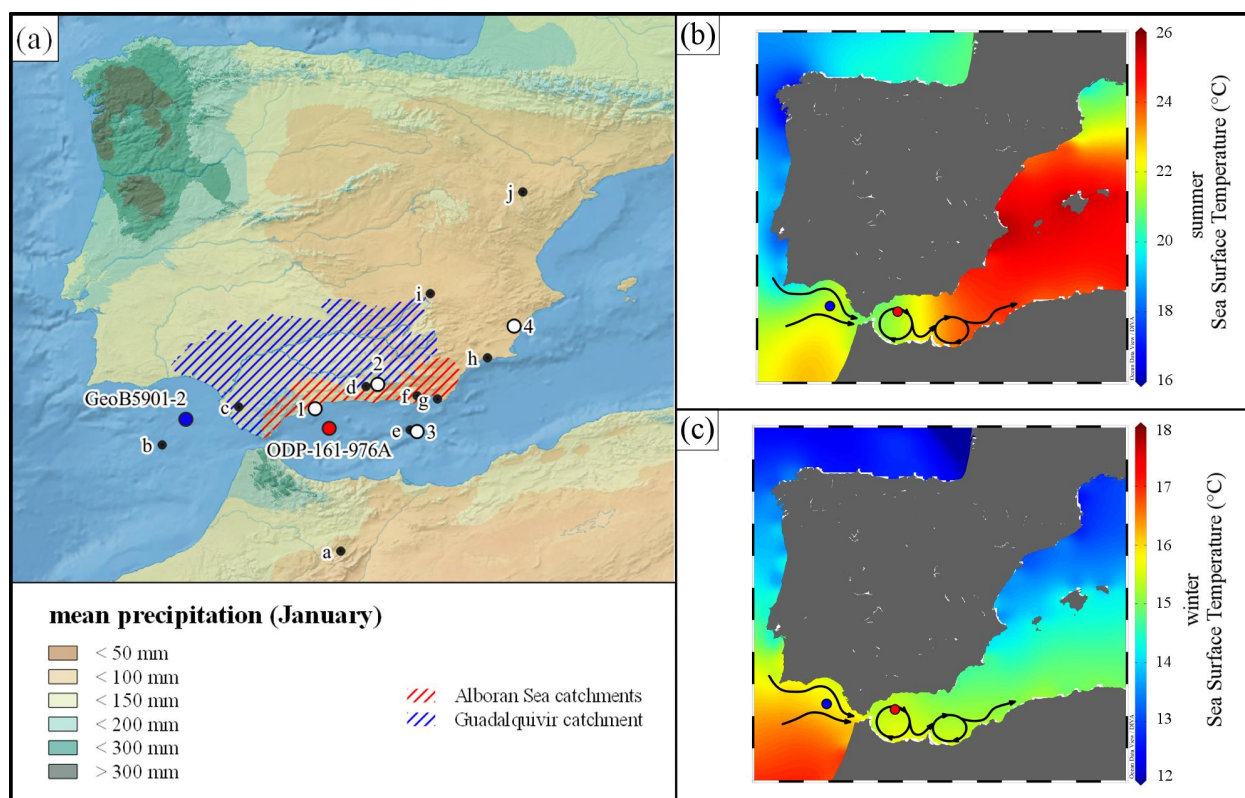Discussions

Figures and tables

Figure 1: Overview maps. (a) overview with discussed (black dots) and shown (white dots) references at the Iberian Peninsula and studied sediment cores. Cores of this study: GeoB5901-2 (blue dot) and ODP-161-976A (red dot). Shown references: 1: El Refugio Cave (Walczak et al., 2015), 2: Borreguil de la Virgen and Borreguil de la Caldera (García-Alix et al., 2018), 3: MD95-2043 (Cacho et al., 2001; Fletcher and Sánchez Goñi, 2008; Martrat et al., 2014; Pérez-Folgado et al., 2003), 4: Elx (Burjachs and Expósito, 2015). Discussed references: a: Grotte de Piste (Wassenburg et al., 2016), b: MD99-2339 (Salgueiro et al., 2014), c: Lake Medina (Schröder et al., 2018), d: Padul (Ramos-Román et al., 2018a,b), e: TTR-293G (Rodrigo-Gámiz et al., 2014), f: San Rafael (Pantaléon-Cano et al., 2003), g: Cabo de Gata (Burjachs and Expósito, 2015), h: Mazarrón (Navarro-Hervás et al., 2014), i: Villaverde (Carrión et al., 2016) and, j: Ejulve cave (Moreno et al., 2017). The main river system and associated catchment of the Guadalquivir (hatched blue area) is shown as well as the river catchments of various small-scale rivers draining the southern Sierra Nevada area (hatched red area). The river catchments have been downloaded from the website of the European Environmental Agency. The colour shading indicates the mean precipitation of January (1970 – 2000) representative of the mean winter season precipitation in the area. The data was provided by WorldClim V2

Climate
of the Past
Discussions

(Fick and Hijmans, 2017). Mean summer (b) and winter (c) SSTs for the period 1955 – 2012 are shown. The data was provided by the World Ocean Atlas 2013 (Locarnini et al., 2013) and processed with Ocean Data View 5.1.2 (Schlitzer, 2018). Black arrows indicate the surface currents in the area including the gyres in the Alboran Sea. Blue and red dot mark locations of sediment cores GeoB5901-2 and ODP-161-976A, respectively.
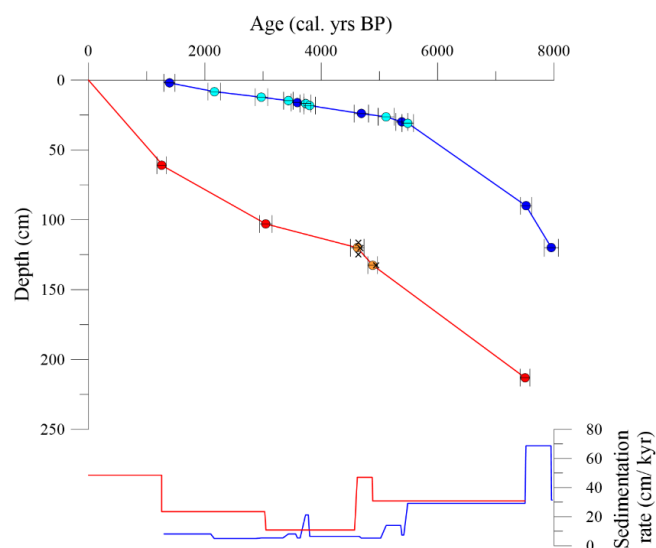

Figure 2: Age model. The age model from ODP-161-976A (red) is based on AMS[14]C dates (red dots) from Combourieu Nebout et al. (2002), which have been re-calibrated by the author and two new AMS[14]C dates from this study (orange dots). Black crosses mark the four AMS[14]C dates of sediment core ODP-161-976A, which are not considered. The Age model of GeoB5901-2 (blue) is based on AMS[14]C datings done by Kim et al. (2004) re-calibrated by the author (dark blue dots) and seven new AMS[14]C dates accomplished during this study (light blue) (for all AMS[14]C datings see Table 1). On the bottom the according sedimentation rates of sediment cores ODP-161-976A (red) and GeoB5901-2 (blue) are shown.
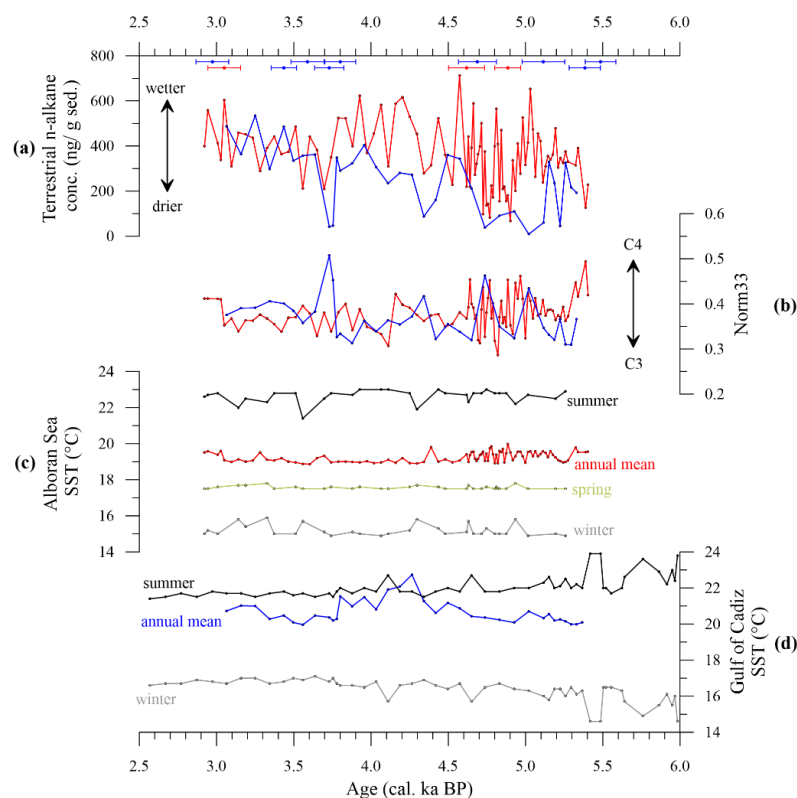
25

30

Figure 3: Data of marine sediment cores ODP-161-976A (red) and GeoB5901-2 (blue). (a) Terrestrial n-alkane concentration (ΣC_{27-33}) indicative of precipitation change. (b) Norm33 n-alkane ratio showing C3 vs. C4 plant input. (c) alkenone and planktic foraminifera based Sea Surface Temperature (SST) reconstruction from ODP-161-976A (black – summer; grey – winter; green – spring; red – annual mean). (d) alkenone and planktic foraminifera based SST reconstruction from GeoB5901-2 (black – summer; grey – winter; blue – annual mean) Coloured dots at the top show AMS[14]C age control points and associated 2σ errors.
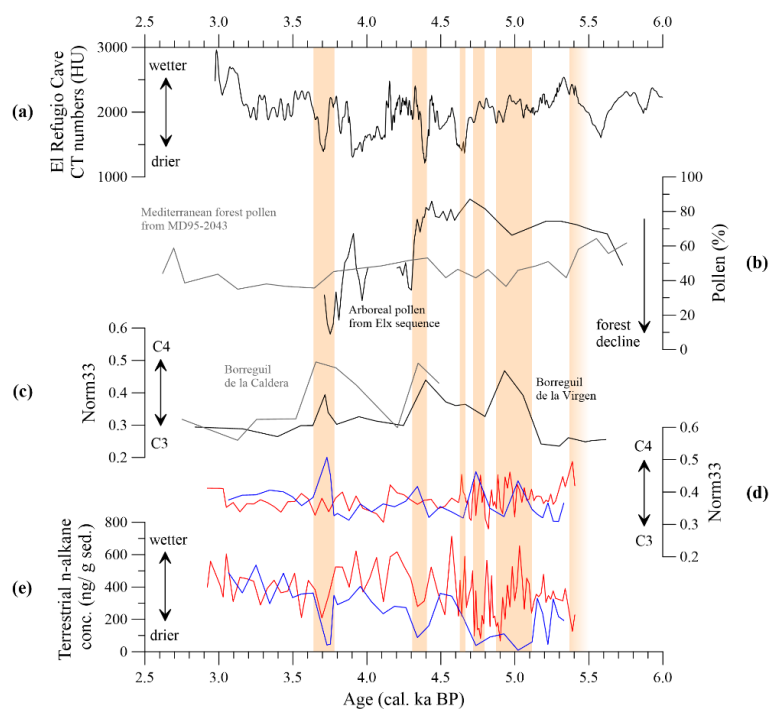
30

24

Figure 4: Proxy data from the Iberian Peninsula. (a) speleothem density data from El Refugio Cave (Walczak et al., 2015) (b) pollen data from Elx sequence (Burjachs and Expósito, 2015; Burjachs et al., 1997) and marine sediment core MD95-2043 (Fletcher and Sánchez Goñi, 2008) (c) Norm33 n-alkane ratios from Borreguil de la Caldera and Borreguil de la Virgen. These data have been calculated on the basis of n-alkane raw data from (García-Alix et al., 2018) (d) Norm33 n-alkane ratios from ODP-161-976A (red) and GeoB5901-2 (blue) (this study) (e) terrestrial n-alkane concentration from ODP-161-976A (red) and Geob5901-2 (blue) (this study). The orange bars indicate dry events recognized in this study. The locations of all the references are shown in Figure 1.
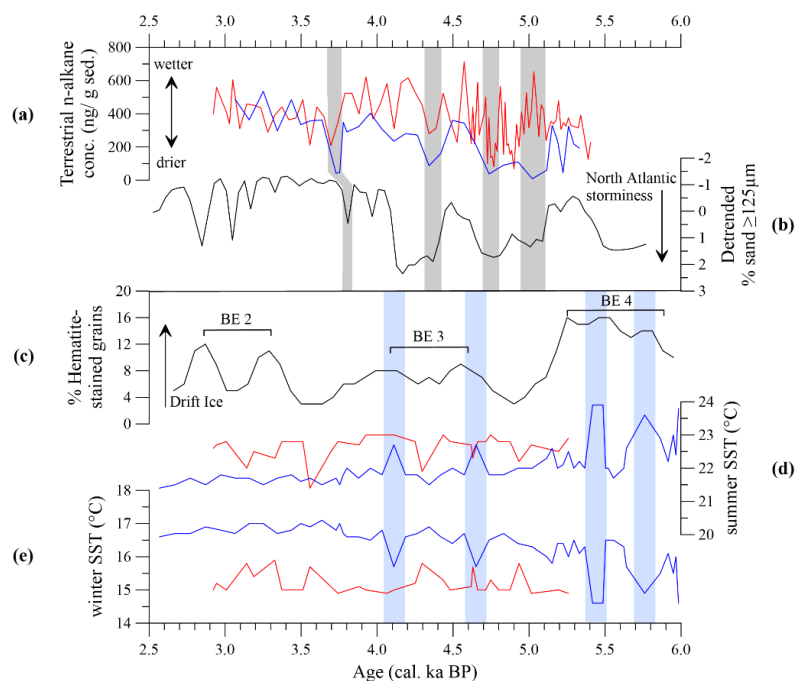
25

25

Climate
of the Past
Discussions

Figure 5: Potential drivers of atmospheric (upper panel) and oceanic (lower panel) climate variability in the Atlantic realm. (a) terrestrial n-alkane concentration from ODP-161-976A (red) and Geob5901-2 (blue) (this study). (b) North Atlantic storminess data of sediment core F06 from Filsø (Denmark) indicative of NAO-like atmospheric variability (Goslin et al., 2018) (c) stacked hematite-stained grain data from the North Atlantic showing the Bond-Events (BE) 2 to 4 (Bond et al., 2001) (d) summer and (e) winter SST from ODP-161-976A (red) and Geob5901-2 (blue) (this study). The grey bars indicate dry events and the blue bars major cooling events in the Gulf of Cadiz recognized in this study.
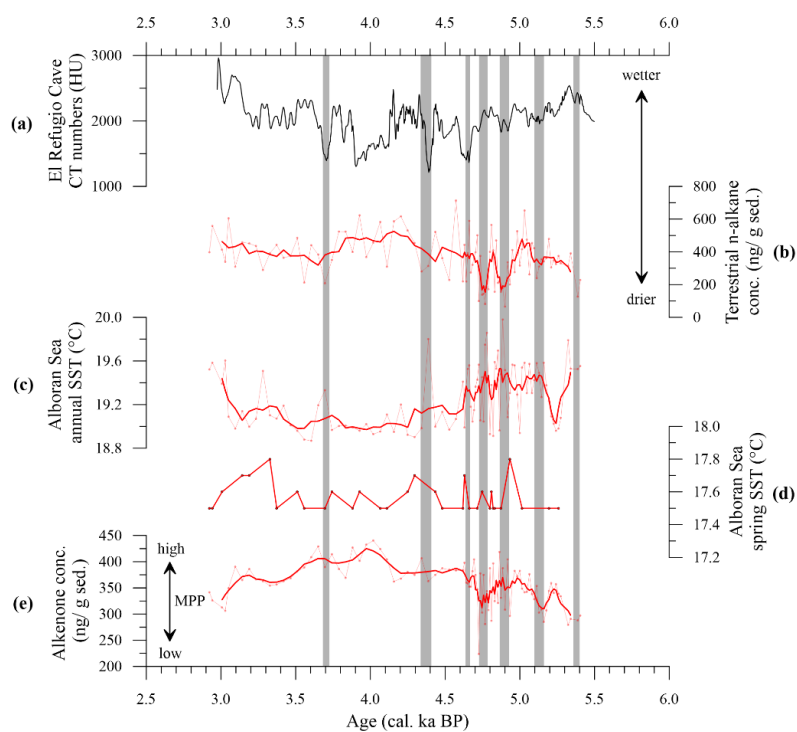
Figure 6: Atmospheric and oceanic variability in the Alboran Sea (ODP-161-976A). (a) speleothem density data from El Refugio Cave (Walczak et al., 2015) (b) terrestrial n-alkane concentration (c) annual mean SST deduced from alkenones (d) spring SST deduced from planktic foraminifera and (e) alkenone concentration indicative of the MPP. Thick red lines in (b), (c) and, (e) are 5-point-running means for better vizualisation, while the raw data is shown in light colors. Grey bars show periods of coupled atmospheric and oceanic variability (i.e. droughts, SST warming and, low MPP) in the Alboran Sea.

25

30

Climate
of the Past
Discussions

Open Access

EGU

Table 1: Age model of sediment cores ODP-161-976 and GeoB5901-2. All dates from previous studies have been re-calibrated. Not considered dates are shown in grey.

Sediment core	Lab. No.	Depth (cm)	AMS^{14}C age (yr BP) ± σ	Calibrated age (yr BP) ± 2σ	Dated material	Reference
GeoB5901-2	KIA-14522	2.00	1840 ± 35	1392 ± 96	planktic mix	(Kim et al., 2004)
GeoB5901-2	KIA-53006	8.25	2485 ± 25	2162 ± 110	*G. ruber* w + p	this study
GeoB5901-2	KIA-53005	12.25	3185 ± 27	2973 ± 106	*G. ruber* w + p	this study
GeoB5901-2	KIA-53002	14.75	3545 ± 26	3436 ± 82	*G. ruber* w + p	this study
GeoB5901-2	KIA-14521	16.00	3685 ± 35	3590 ± 108	planktic mix	(Kim et al., 2004)
GeoB5901-2	KIA-53003	16.75	3789 ± 27	3730 ± 95	*G. ruber* w + p	this study
GeoB5901-2	KIA-53004	18.25	3852 ± 27	3801 ± 100	*G. ruber* w + p	this study
GeoB5901-2	KIA-14520	24.00	4500 ± 40	4689 ± 123	planktic mix	(Kim et al., 2004)
GeoB5901-2	KIA-52665	26.25	4820 ± 35	5116 ± 138	*G. ruber* w + p	this study
GeoB5901-2	KIA-14518	30.00	5035 ± 40	5384 ± 101	planktic mix	(Kim et al., 2004)
GeoB5901-2	KIA-52666	30.75	5130 ± 40	5486 ± 99	*G. ruber* w + p	this study
GeoB5901-2	KIA-14516	90.00	7035 ± 55	7518 ± 97	planktic mix	(Kim et al., 2004)
GeoB5901-2	KIA-13704	120.00	7495 ± 50	7955 ± 121	planktic mix	(Kim et al., 2004)
ODP-161-976C	KIA-6435	61.00	1710 ± 40	1259 ± 82	*G. bulloides*	(Combourieu Nebout et al., 2002)

ODP-161-976C	KIA-6436	103.00	3235 ± 30	3050 ± 106	*G. bulloides*	(Combourieu Nebout et al., 2002)
ODP-161-976A	KIA-53326	116.25	4435 ± 35	4636 ± 138	*G. bulloides*	this study
ODP-161-976A	KIA-53235	120.25	4435 ± 30	4619 ± 117	*G. ruber* w + p	this study
ODP-161-976A	KIA-53327	120.25	4480 ± 40	4671 ± 130	*G. bulloides*	this study
ODP-161-976A	KIA-53236	124.75	4435 ± 35	4636 ± 138	*G. ruber* w + p	this study
ODP-161-976A	KIA-53234	132.75	4650 ± 35	4885 ± 84	*G. ruber* w + p	this study
ODP-161-976A	KIA-53325	132.75	4700 ± 50	4945 ± 134	*G. bulloides*	this study
ODP-161-976C	KIA-6437	213.00	7010 ± 50	7500 ± 84	*G. bulloides*	(Combourieu Nebout et al., 2002)